Dye Encapsulation in Polynorbornene Micelles

Nia C. Bell[1], **Samantha J. Doyle**[1], **Giulia Battistelli**[2], **Clare L. M. LeGuyader**[1], **Matthew P. Thompson**[1], **Ambata M. Poe**[3], **Marco Montalti**[2], **S. Thayumanavan**[3], **Michael J. Tauber**[1], and **Nathan C. Gianneschi**[1,*]

[1]Department of Chemistry & Biochemistry, University of California San Diego, 9500 Gilman Drive, MC 0343, La Jolla, CA, 92093, USA

[2]Department of Chemistry "G. Ciamician", University of Bologna, Via Selmi 2, Bologna, Italy

[3]Department of Chemistry, University of Massachusetts, 710 North Pleasant Street, Massachusetts 01003-9336, USA

Abstract

The encapsulation efficiency of high-T_g polynorbornene micelles was probed with a hydrophobic dye 2,6-diiodo boron-dipyrromethene (BODIPY). Changes in the visible absorption spectra of aggregated versus monomeric dye molecules provided a probe for assessing encapsulation. Polynorbornene micelles are found to be capable of loading up to one BODIPY dye per ten polymers. As the hydrophilic block size increased in the polymeric amphiphiles, more of the dye was incorporated within the micelles. This result is consistent with the dye associating with the polymer backbone in the shell of the micelles. Encapsulation rate varied significantly with temperature, and a slight dependence on micellar morphology was also noted. Additionally, we report a 740 µs triplet lifetime for the encapsulated BODIPY dye. The lifetime is the longest ever recorded for a BODIPY triplet excited state at room temperature, and is attributed to hindered triplet-triplet annihilation in the high viscosity micellar shell.

Graphical Abstract

---
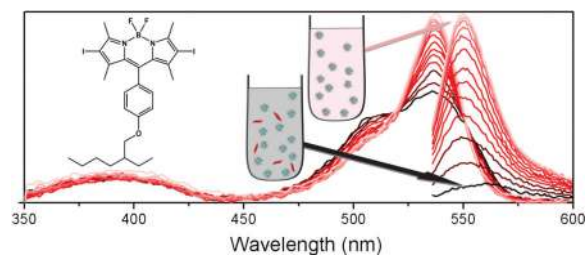
*Corresponding Author ngianneschi@ucsd.edu.

Keywords

BODIPY; iodinated BODIPY; halogenated BODIPY; ROMP; diblock copolymer; micelle; nanoparticle; encapsulation rate; encapsulation efficiency; dye disaggregation; glassy core; high T_g; morphology; transient absorption spectroscopy; triplet excited state

Introduction

Self-assembled block copolymers are an important family of synthetic nanomaterials with complex architectures and chemical functionalities programmable through the design of the constituent molecular components.[1–4] They are central to emerging biomedical applications where therapeutic, contrast, and targeting agents may be polymerized, conjugated or non-covalently encapsulated in a controlled and modular manner.[5–8]

Amphiphilic diblock copolymers are driven to assemble in aqueous solutions because of the hydrophobic effect. The morphology adopted by the assembled micelle has a subtle dependence on inter- and intramolecular interactions, interfacial tension between the core and the solvent, and core stretching.[3, 9] Self-assembled polymers with high glass transition temperatures (T_g), such as polynorbornene, polystyrene and poly(methyl methacrylate), can form kinetically-trapped nanostructures.[10] The stability of these nanostructures is excellent, but their ability to incorporate drug molecules after micelle formation may be poor, because of the glassy nature of their cores. Although low encapsulation efficiencies are expected of polynorbornene micelles, this family of block copolymers was investigated because they are the product of the highly versatile ring-opening metathesis polymerization (ROMP) strategy.[3, 5–6, 11] The ability of polynorbornene nanomaterials to load hydrophobic molecules is a relatively unexplored topic, motivating our interest in this specific polymer. Notable exceptions include covalent indomethacin incorporation and cobalt ion complexation in the hydrophobic cores of polynorbornene micelles, and an example of steroid attachment and release from polynorbornene films.[12–14] We reasoned that if the loading of drug-like molecules were understood, it could be optimized, and that such a strategy would provide a flexible and straightforward way to package guest molecules for delivery in applications including therapeutic and diagnostic targeting.[5]

Measurement of pyrene emission is the most established method for assessing the ability of micelles to act as nanocarriers for non-covalently loaded hydrophobic drugs.[15–18] The fluorescence from this probe allows assessment of the partition coefficient and the characteristics of the local environment (core or shell) around the probe within the micelle.[17, 19] Pyrene is also used to measure the critical micelle concentration (c.m.c.) of micelle solutions.[4] However, we have found it impossible to characterize the micelle/guest interactions via standard pyrene analysis for the types of polynorbornene micelles reported herein. For that reason and others detailed below, we investigated 2,6-diiodo BODIPY as a probe for micellar guest uptake.

The BODIPY, or boron-dipyrromethene, family of dyes have been explored for diverse applications, including for lasers[20] and OLEDs; for solar energy conversion;[21] as sensitizers in photodynamic therapy;[22–24] and as sensors of pH, nitric oxide, heavy metals and solvent

polarity.[25–26] This versatility stems in part from the ease of tuning the photophysics or reactivity of BODIPY via synthetic modifications. Derivatives similar to the one investigated in our study, (2,6-diiodo BODIPY depicted in Figure 1), have been explored as possible photosensitizers for solar hydrogen production and triplet-triplet annihilation (TTA) upconversion because of their intense absorbance in the visible part of the spectrum, good photostability, and high yield of long-lived triplet excited states.[27–28]

An iodinated BODIPY derivative was chosen as the probe in this study because it has several spectroscopic and photophysical properties that can be used to monitor micelle encapsulation. First, there are changes in the absorption spectrum of BODIPY that reflect the aggregation state of the molecule before and after incorporation. We proposed to use these aggregation-dependent signatures to quantify micelle-encapsulation of the dye. Our approach was partially inspired by an example where spectral signatures of BODIPY dye aggregation and disaggregation were used as a read-out in a chemical assay, and another example where they were used to monitor lower critical solution temperature (LCST) behavior in polymeric materials.[29–30] Second, we expected the triplet excited state lifetimes of BODIPY encapsulated by polynorbornene micelles to be higher than when dispersed in solvents, because the high viscosity polymer reduces the rate of various quenching reactions. We selected the 2,6-diiodo BODIPY molecule because the heavy-atom substituents enhance the formation of triplet excited states for the latter studies. [23, 31]

Materials and Methods

The 2,6-diiodo BODIPY molecule (M_w = 704.2 g.mol^{-1}) was synthesized according to a procedure described previously.[32] It was stored as a dry powder in the dark under ambient conditions. The molar absorptivity of the molecule in acetone was measured to be 82,000 M^{-1} cm^{-1}, consistent with values reported for similar molecules.[23, 33–34]

The reagents used in polymer synthesis and micelle formation were purchased from commercial sources and used without further purification. Norbornene monomers suitable for ring opening metathesis polymerization (ROMP) substituted with either a phenyl or short PEG moiety,[35–36] and the ROMP initiator [(IMesH$_2$)(C$_5$H$_5$N)$_2$(Cl)$_2$Ru=CHPh],[37] were synthesized according to literature procedures. Polymerizations were performed in anhydrous dichloromethane (DCM) under an inert atmosphere of dinitrogen (N$_2$). For a typical polymer synthesis ((PEG)$_4$)$_m$-**b**-(phenyl)$_n$ a 1 mL solution of the (PEG)$_4$ monomer at a concentration (*c*) in the range 50 – 100 mM, was stirred at room temperature and a solution of the initiator (also in anhydrous DCM) was added quickly to a final concentration of *c/m* mM. An aliquot of approximately 5% of the solution was removed after 20 minutes and a molar excess of ethyl vinyl ether added in order to obtain the homopolymer for characterization of the first block. The phenyl monomer was added to the remaining reaction mixture to obtain a final concentration of (*c* × *n*)/*m* mM and the solution left stirring at room temperature for a further 20 minutes. Following ethyl vinyl ether termination of the diblock copolymer reaction mixture the product was precipitated twice in 30 mL of a cold 1:1 methanol:diethyl ether solution and dried in a desiccator.

Measurement of polymer molecular weight (M_N) and dispersity (M_W/M_N) was performed using size exclusion chromatography with multi-angle light scattering (SEC-MALS). The columns were Phenomenex Phenogel 5u 10, 1K–75K, 300 ×7.80 mm in series with a Phenomex Phenogel 5u 10, 10K–1000K, 300 × 7.80 mm (0.05 M LiBr in DMF), and the pump was a Shimadzu LC-AT-VP. The light scattering setup included a multi-angle light scattering detector (DAWN-HELIOS: Wyatt Technology), a refractive index detector (Wyatt Optilab T-rEX) and a UV-Vis detector (Shimadzu SPD-10AVP). The system was calibrated with a polystyrene standard. The *dn/dc* values for (PEG)$_4$ and phenyl homopolymers in DMF were measured, and are 0.100 and 0.179 mL/g respectively. These values allow the molecular weight and dispersity of the first polymerized block to be determined with good certainty. In the case of the diblock copolymers, for which the *dn/dc* was not measured, the molecular weight was instead determined with ^{1}H- NMR spectroscopy (Varian Mercury Plus spectrometer, 400 MHz). The signals from phenyl protons of the hydrophobic block were integrated relative to the olefin protons on the polymer backbone. The total degree of polymerization and molecular weight of the second polymerized block was determined using NMR data along with the molecular weight of the first polymerized block, as measured by SEC-MALS. Chemical shifts (^{1}H) are reported in (ppm) relative to the residual protonated solvent peak.

The amphiphilic diblock copolymer micelles were formed using the solvent switch method.[3] Initially the polymer was dissolved in a cosolvent that solubilized both blocks, at a concentration of 1 mg/mL. The cosolvent was either dimethyl sulfoxide (DMSO), *N*-*N′*-dimethyl formamide (DMF), acetonitrile (ACN) or tetrahydrofuran (THF). A 1:1 cosolvent:H$_2$O mixture was added to the polymer solution with a syringe pump (rate controlled over a 10 mL/hr and 360 mL/hr range) until the volume doubled. The diblock copolymer micelles are expected to be kinetically trapped in a binary solvent mixture having a water concentration of 25% v/v.[38] The solution was stirred for 10 minutes at room temperature, then transferred to 3,500 MWCO tubing (Snakeskin), and dialyzed against 2 L of deionized water for two days with at least three exchanges of water.

The concentration of the aqueous solutions of assembled nanostructures was determined with a calibration curve that was generated for each polymer. The dry polymer was carefully weighed, dissolved in HPLC-grade ACN, and a serial dilution yielded a linear relationship between concentration and the absorbance at 250 nm (Figure S1). The absorbance at 250 nm is attributed mainly to the phenyl chromophore and, to a lesser extent, the imide group in the PEG-succinimide. To measure the concentration of the aqueous polymeric solutions, a known volume was first lyophilized and then resuspended in ACN.

Steady state absorbance was measured with a Cary 100 Bio UV-Vis spectrophotometer (Varian) equipped with a Peltier temperature control accessory. A spectrofluorometer (PTI) was used to measure fluorescence, and quantum yields were compared with rhodamine 640 perchlorate in methanol as a standard. In Figures 4 and S9 where absorbance and fluorescence spectra were recorded every 10 minutes for several hours, a multimode plate reader (EnSpire, Perkin Elmer) was employed.

The microsecond transient absorption (μs-TA) kinetics and spectra were acquired with a custom system.[39] The pump wavelength was 537 nm. The power at the sample was 100 μJ/ pulse. The time response of the detection system was approximately 30 ns. The data were recorded every 10 nm, from 300 to 700 nm. The 540 nm wavelength was excluded because of scattering from the pump. 1000 kinetics were averaged at each wavelength. Solutions of 2,6-diiodo-BODIPY in toluene were prepared and sealed in an argon-filled glovebox. The aqueous micelle sample for μs-TA was bubbled with N_2 for one hour directly before the measurement. This method of deoxygenation avoided aggregation that would otherwise occur with drying and re-suspension of the micelles. The maximum absorbance of the samples for μs-TA was 0.2 (1 cm path length). Solutions were stirred throughout the pump-probe spectroscopy, and sample degradation, monitored by UV-Vis spectra before and after irradiation, was at most 11% in toluene and 6% in micelles. The decay kinetic at 440 nm (maximum of triplet absorption) was remeasured at the end of the run to verify that the cuvettes remained sealed and oxygen-free for the duration of the experiment. The data were smoothed using a 15 point boxcar algorithm and fitted with exponential functions (OriginPro 8 software).

Transmission electron microscopy (TEM), atomic force microscopy (AFM), and dynamic light scattering (DLS) were carried out to assess the morphology and dispersion of the aqueous self-assembled nanostructures. Unstained dry-state TEM was carried out on a FEI Tecnai G2 Sphera with acceleration voltage of 200 KV. Samples were prepared by glow discharge of carbon grids, upon which 3.5 μL of the solution was deposited. After a 5 minute wait, the grids were rinsed with three drops of deionized water, and excess liquid was wicked away with filter paper. AFM images were acquired on a Bruker Dimension Icon AFM using a ScanAsyst silicon nitride probe and processed using Nanoscope 9.1 software. Samples were dropped onto glow discharged mica surfaces, then allowed to sit for 5 minutes before excess liquid was wicked away. For DLS (DynaPro Nanostar, Wyatt) 0.4 mg/mL aqueous solutions of nanostructured polymer were diluted by a factor of 10 with deionized water before measurement.

A 2,6-diiodo BODIPY crystal of sufficient size for single crystal x-ray diffraction (XRD) was obtained by slow evaporation from pentane at room temperature. The measurement was carried out on a Bruker Kappa APEX-II CCD diffractometer with Mo K_α radiation (λ= 0.71073 Å).

Results and Discussion

The main features in the ultraviolet-visible spectrum of the alkoxy-phenyl 2,6-diiodo BODIPY molecule in acetone (Figure 1) are a broad $S_0 \rightarrow S_2$ absorption centered at 390 nm, and a narrower $S_0 \rightarrow S_1$ band with maximum at approximately 530 nm. A shoulder on the shorter wavelength side of the main peak (circa 505 nm) is attributed to the 0–1 vibrational band of the same transition. The shape of the fluorescence emission is approximately a mirror image of the $S_0 \rightarrow S_1$ absorption, and the Stokes shift is small (18 nm, or 630 cm^{-1}). The fluorescence quantum yield in acetone was 0.03, in good agreement with values reported for similar diiodo BODIPY molecules.[28, 34]

When dissolved in different organic solvents at a concentration of 10 μM, subtle changes in the absorption spectra of the 2,6-diiodo BODIPY dye were noted. The ratio of the amplitudes of the 0–0 and 0–1 bands of the $S_0 \rightarrow S_1$ electronic transition, referred to as A_{ratio}, was found to depend only slightly on solvent polarity, but not on proticity or viscosity (Figure S2). For convenience in the analysis of the A_{ratio}, we assess the amplitude of the 0–1 band at a position that is 27 nm blue-shifted from the wavelength of maximum absorbance. The fluorescence (Stokes shift and emission intensities) also depended slightly on the solvent, but these changes played little role in our analysis.

The dye is insoluble in pure water, but water mixed with small amounts of a miscible organic solvent that dissolves BODIPY, such as acetone, yielded stable solutions of dye aggregates. A solvent ratio of 3 % v/v acetone /water (Figure S3) was employed in all subsequent experiments. The absorption spectrum of BODIPY in this binary solvent system was broader, and had a much lower A_{ratio} (≈ 1.2) than the solvated dye in pure organic solvents ($A_{ratio} = 2.5 – 3.3$), see Figure 2(a). The solution also had very low fluorescence emission. These spectral and photophysical changes are typical characteristics of H-aggregates.[40–41] Similar changes have been reported for dimers of BODIPY in cofacial arrangements.[42–46]

From the A_{ratio} value measured in the 3 % v/v acetone in water binary solution (≈ 1.2), and a 10-fold decrease in fluorescence quantum yield relative to dye in pure acetone, we conclude that there is an insignificant amount of monomeric dye in the binary solution. The BODIPY dye aggregates, which dominate in the 3 % v/v acetone/water solution, were characterized by DLS, dry-state TEM, and X-ray diffraction. The results from DLS, and images from TEM are consistent with particulates of BODIPY that have sub-100 nm dimensions, and crystalline nanostructures (Figure 2). Single-crystal X-ray diffraction reveals that the 2,6-diiodo BODIPY molecule pack in dimeric units in an anti-parallel arrangement. Anti-parallel stacking is energetically more favorable than parallel, because the latter arrangement would require a sterically-hindered rotation of the *meso*-phenyl relative to the plane of the BODIPY core.

The aggregation-dependent A_{ratio} signature of the absorption spectrum was next used to probe the encapsulation of BODIPY by polynorbornene nanostructures. We investigated the effect of polymer hydrophobicity and micelle morphology on the encapsulation efficiency, and rate of dye incorporation. Encapsulation efficiency is defined as the percentage of dye in a sample encapsulated by the micelles, relative to the total dye in solution. For this study, a series of diblock copolymers were synthesized with different proportions of hydrophilic to hydrophobic blocks ($X_m = m/(m+n)$) where m and n are the degree of polymerization of the $(PEG)_4$ monomer and phenyl monomer respectively. Details of the polymer characterization are included in Figures S4 and S5 and summarized in Table 1.

When transitioned from THF, a good solvent for both the phenyl and $(PEG)_4$ blocks in the polymers, into water (a selective solvent), polymers A to D formed small spherical nanoparticles of similar size to one another (Figures 3 and S6). The particles of polynorbornene had sufficient electron density to be imaged unstained in dry-state TEM. It is plausible, given their size, that the nanoparticles are simple micelles with a core

comprised largely of the hydrophobic block, and a shell rich with the hydrophilic block. The kinetically trapped structures allow access to different morphologies by slight changes in preparation conditions.[3] For example, spherical or worm-like micelles of polymer B can be formed by varying the organic solvent (Figure S7). This set of polymer B nanostructures was used to investigate the effect of micelle morphology on dye encapsulation, as described below.

The partitioning of 2,6-diiodo BODIPY from an aggregated state in water to the micelle environment was tested by monitoring a solution where both aggregates and micelles were present in a binary solution of acetone/water (3 %v/v). An increase in fluorescence emission from the sample, along with a linearly-correlated increase in A_{ratio}, are consistent with the disaggregation of the aqueous H-aggregates in favor of dispersed dye monomers in the micelles (Figure 4). We confirmed that the ratio of the band amplitudes (A_{ratio}) is proportional to the area ratio of the fitted Gaussian functions (Figure S8). To ensure that the spectral changes observed were a result of interactions between the dye and the micelles an analogous experiment without the micelles present was carried out as a control. Whether the fluorescence intensity or the shape of the absorbance spectrum of the dye changed over time without the micelles present was investigated (Figure S9). We also checked that neither dye encapsulation nor heating (50 °C for one hour) induced changes in micelle morphology (Figure S10).

The micelles formed from polymers A to D were then used to investigate the effect of temperature on encapsulation efficiency, and the rate of dye incorporation (Figure 5). The polymer E micelles were excluded from this study and others involving heating, because of their tendency to transform from sphere to worm-like micelles at elevated temperatures (Figure S11). In our experience, more hydrophilic polymers ($X_m > 0.7$) than polymer E did not self-assemble into stable micelles. At a fixed polymer concentration (0.2 mg/mL) and weight ratio of dye to polymer (0.02), A_{ratio} was monitored at temperatures between 30 and 60 °C for the polymer A micelles and between 40 and 60 °C for the remaining micellar samples. The change in A_{ratio} over time was well described by a single exponential function with a rate constant (k) and offset (y_0) related to the encapsulation rate and efficiency respectively. A further experiment, as described below, is required to determine the factor that maps y_0 to encapsulation efficiency. At the dye-to-polymer mass ratio investigated y_0 was found to be temperature independent with $A_{ratio} = 2.5 \pm 0.1$ for all micelles at all temperatures. Encapsulation rate, on the other hand, increased with temperature and the linearity of the Arrhenius plot indicated that a single thermally activated process dominated the encapsulation kinetics in the range investigated. No significant changes in encapsulation rate due to hydrophilicity of the polymer in the micelles were evident from this study.

To quantitatively relate A_{ratio} to encapsulation efficiency, it was necessary to determine its value when the dye was completely dispersed in the micelles. From the solvent polarity screen (Figure S2), we expected the A_{ratio} to be in the range of 2.5–3.3. However, a direct measurement was performed as follows: for micelles of polymers A to D, solutions with varying ratios of dye to polymer were incubated at 50 °C for 1 hour before their A_{ratios} were recorded. After this length of time at 50 °C we were confident that the system reached equilibrium, in view of the temperature dependence described above. This experiment also

allowed assessment of dye-to-polymer ratios for which the A_{ratio} metric could serve as an indicator of the dye state (i.e. aggregated, or incorporated).

As seen in Figure 6(a), at low BODIPY to polymer molar ratios, the regime where all of the dye is expected to be encapsulated, A_{ratio} saturates at 3.0 ± 0.1. At high BODIPY to polymer ratios, where aggregates in the aqueous phase dominate, A_{ratio} was found to be 1.23 ± 0.03. The data were fitted to a derivation of the Hill equation which scales the function between a lower bound (y_0) and upper bound (y_1):

$$y = y_1 + (y_1 - y_0)\frac{x^n}{(k^n + x^n)} \quad \text{(Equation 1)}$$

where x is the molar ratio; k is the molar ratio at the midpoint of the curve; and n is the Hill coefficient. This Hill function was chosen as it can be used to assess the cooperativity of binding events. Interestingly, the positive Hill coefficients extracted from these fits, $n = 1.5$ ± 0.2, suggest that the binding of dye to the micelles acts to increase the affinity of the micelles for other dye molecules. In situations where the micelles are in equilibrium with BODIPY aggregates, A_{ratio} can be an indicator of the aggregation state of 2,6-diiodo BODIPY over a large range of dye to polymer concentrations (two orders of magnitude). From Figure 6 (a) and a rough approximation of the aggregation number of the micelles the maximum loading of the micelles can also be estimated to be one dye molecule per ten polymers, or 10–30 dye molecules per micelle.

The encapsulation efficiency (EE) of the micelles can be calculated from A_{ratio} using the straightforward empirical relation, which incorporates the fitted lower and upper limits for A_{ratio}:

$$EE = \left(\frac{A_{ratio} - y_0}{y_1 - y_0}\right) \times 100\% \quad \text{(Equation 2)}$$

A linear relationship between encapsulation efficiency and A_{ratio} is consistent with the linear correlation of A_{ratio} with fluorescence intensity (Figure 4 (d)). Both of these spectroscopic characteristics quantify the monomeric (encapsulated) dye population.

The higher dye encapsulation of the more hydrophilic polymers, inferred from the shift to the right of the data in Figure 6 (a), was intriguing. The A_{ratio} data were replotted versus the molar ratio of dye to phenyl monomer (Figure 6 (b)) and dye to (PEG)$_4$ monomer (Figure 6 (c)). This analysis negated the influence of polymer molecular weight on the data, and allowed the contributions of both blocks on dye encapsulation to be distinguished. In Figure 6 (b) points with the same x-axis coordinate have the same ratio of dye to phenyl monomer. If the encapsulation efficiency were solely determined by the amount of phenyl monomer in solution, we would expect the data from the different polymers to overlap on this scale. Instead, a systematic shift to the right with increasing polymer hydrophilicity (X_m) is observed. Confirmation that the (PEG)$_4$ monomer dominated the phenyl monomer in determining the encapsulation efficiencies of the micelles was found with the near perfect

overlap of the data from the four polymeric micelles (A to D) in Figure 6 (c). The k parameters in the Hill fits of the data in Figures 6 (b) and (c) are plotted in Figure S13.

These data suggests that micelle encapsulation of the 2,6-diiodo BODIPY molecule is driven by interactions with the $(PEG)_4$ block, but not the phenyl block, of the polymers. This initially surprising result can be rationalized if the glassiness of the micellar cores is considered. With a T_g of 120 to 150 °C, polynorbornene phenyl homopolymers (4 to 50 kDa) are effectively frozen in the core, and therefore unable to rearrange to support dye encapsulation.[3] Extremely poor permeability of bulk polynorbornene has been reported, even to gases, and attributed to the strong intermolecular interactions, and therefore low fractional free volume.[47]

To determine whether the poly(ethylene) glycol or polymer backbone portion of the shell was primarily responsible for solubilizing the dye, the relationship between relative dye/ $(PEG)_4$ concentration and A_{ratio}, for a regular 4.6 kDa poly(ethylene) glycol molecule $(PEG_{4.6kDa})$ and a ROMP homopolymer of $(PEG)_4$ $(Homo-(PEG)_4)$, was investigated (Figure 6 (c)). We calculated that the $PEG_{4.6kDa}$ molecule had an equivalent of 19 $(PEG)_4$ units. No change in the A_{ratio} of the dye with concentration of $PEG_{4.6kDa}$ was observed with or without heating at 50 °C for one hour (data without heating shown in Figure 6 (c)). However, in the presence of the $Homo-(PEG)_4$ an immediate and concentration dependent increase in the A_{ratio} of the dye at room temperature occurred. Micelle formation in these solutions was not expected, nor was it observed by DLS or TEM, indicating that $Homo-(PEG)_4$ is completely dispersed at room temperature in the concentration range of interest (cloud point of the most concentrated polymer solution ≈ 35 °C (Figure S14)).[48] Thus the interaction of the dye with $Homo-(PEG)_4$ but not with $PEG_{4.6kDa}$ points to the polynorbornene backbone in the $(PEG)_4$ block as an important factor in determining dye encapsulation by the micelles. Through this study we have demonstrated that non-covalent encapsulation of a hydrophobic molecule post micelle formation is determined by the proportion of hydrophilic block, i.e. the amount of polymer not frozen in an amorphous glassy core. This knowledge will allow for more rational design of these nanomaterials for drug loading applications.

There are significant differences between the interaction of the dye with the micelles (A to D) and $Homo-(PEG)_4$, namely the lack of temperature dependence and the shift to an approximately 300 times lower dye-to-polymer concentration in the case of the dispersed polymer. The difference in the relative polymer concentration required to encapsulate the same amount of dye in both cases can be explained if the local $(PEG)_4$ concentrations in the micelle sample are considered. Using rough values for micelle diameter (30 nm to 50 nm), aggregation number (100 to 300), and the molar volume of the phenyl (205 cm^{-3}) and $(PEG)_4$ (305 cm^{-3}) monomers, the local concentration of $(PEG)_4$ in the micellar shell was indeed approximately 300 times higher than the global solution concentration. Thus, the partitioning of 2,6-diiodo BODIPY from the aqueous phase into the polymer is driven by the local density of polynorbornene-$(PEG)_4$.

The temperature dependence of dye encapsulation by micelles, as opposed to the dispersed $Homo-(PEG)_4$ polymer, suggests that the predominant energy barrier overcome by heating is

related to the ability of the dye molecule to access the micelle shell rather than diffusion or dye solubility. The $(PEG)_4$ block in the shell of the micelle represents a significantly more constrained and dense environment than Homo-$(PEG)_4$ polymer dispersed in solution, so it is not surprising that the interactions between the polynorbornene-$(PEG)_4$ and 2,6-diiodo BODIPY molecule are different in both cases. The water solubility of $(PEG)_4$ in the micelles decreases with increasing temperature as a result of lower critical solution temperature (LCST) behavior, see Figure S14. The polar group dehydration and collapsed conformation of PEG above its LCST would increase the hydrophobicity of the micelle shell and its amenability to interact with large hydrophobic dye molecules. Polymer mobility in the micellar shell, because of $(PEG)_4$ moieties shielding the intermolecular interactions, facilitates dye encapsulation. Micellar shells are often described in terms of an inner corona (or interfacial region) and outer corona (or shell-water interface). This approach takes into account the radial distance dependent densities that determine the properties of the shell.[10] We will return to this description of a micelle shell when interpreting the excited-state lifetimes of the encapsulated BODIPY dyes.

To ensure that the slight differences in the size of the micelles used in the previous study (polymers A to D) could not have interfered with the results, the effect of micelle size and morphology on encapsulation rate and efficiency of the 2,6-diiodo BODIPY molecule with polymer B was briefly investigated. A diverse range of micelle morphologies were synthesized from polymer B (see Figure S7), including larger spheres (some of which may have been vesicle-like) and worms. The micelles were then incubated at 50 °C with the dye, at a fixed molar ratio with the polymer. We found that the equilibrium A_{ratio} was independent of morphology (= 2.70 ± 0.08). However, the rate of encapsulation varied, and was approximately 100 % slower in the worm-like micelles and 35 % slower in the smallest spherical micelles compared to the largest spherical micelles, see Figure S7. The lack of correlation between encapsulation rate and the surface area to volume ratio of the nanomaterials, supports our hypothesis that mobility and/or packing of the $(PEG)_4$ block, not dye solubility and diffusion, is the primary factor governing dye encapsulation.

The majority (> 95 %) of the photons absorbed by 2,6-diiodo BODIPY generate long-lived triplet excited states, because intersystem crossing is enhanced via the heavy-atom effect. The photophysics of the triplet excited state provides a sensitive way to monitor the micelle encapsulation. Therefore we carried out a preliminary investigation, using microsecond transient absorption (μs-TA) spectroscopy. The smallest micelles, 15–20 nm diameter ones of polymer E were used in the μs-TA experiment to minimize laser scattering (Figure S5). Dye molecules in a molar ratio of 0.05 per polymer were incubated at 35 °C for 48 hours, then concentrated (using a SpeedVac™) to obtain 4 mL of a 78 μM polymer solution. A 2.5 μM solution of 2,6-diiodo BODIPY in HPLC grade toluene was also prepared.

The A_{ratio} of 2,6-diiodo BODIPY was approximately 3 in both the toluene and micellar samples, indicating that all the dye in the latter was encapsulated and monomeric. The profiles of the μs-TA spectra of 2,6-diiodo BODIPY in toluene and aqueous micelles are similar (Figure 7), with a triplet state absorption band at approximately 450 nm and the ground state bleach at 530 nm. There is a weaker absorption band with maximum >650 nm which is similarly assigned to the triplet state.[34] In toluene the kinetics of the 2,6-diiodo

BODIPYs triplet state is mono-exponential with a characteristic lifetime, τ_t, of 410 ± 30 μs. A literature value of τ_t for a similar 2,6-diiodo BODIPY molecule in toluene at 1 μM is shorter than ours at 229 μs.[33] It is possible that the alkoxy-phenyl substituent, specific to the 2,6-diiodo BODIPY of our study could slow TTA via steric effects. In the micelles, the triplet excited state of BODIPY decays bi-exponentially. One possible interpretation of the two decay components is that 72 ± 6 % of the BODIPY molecules are in an environment that supports a long lifetime($\tau_t = 740 \pm 70$ μs), and the remainder are quenched ($\tau_t = 14 \pm 4$ μs). To determine the characteristic triplet lifetimes and associated uncertainties reported above all data points from the decay of the triplet state and recovery of the bleach, with signal to noise greater than 10, were used. The lifetime was taken as the average of these values and the standard deviation, the uncertainty. Although the presence of further transient species cannot be completely ruled out, because of the size of these uncertainties, no specific spectral feature attributable to the formation of any significant intermediate can be evidenced by spectral analysis. Moreover no improvement in the fitting of the experimental data was achieved by using more complex kinetic models.

Reduced TTA can explain the exceptionally long triplet lifetime that was the majority component found for the kinetic decay of 2,6-diiodo BODIPY molecules in the micelle samples. The good separation of the dye in the micelles (as reflected by the monomeric absorption spectrum and loading of one dye molecule per ten polymers) and the high micro-viscosities within polynorbornene-dense environments are expected to hinder TTA events.[49] To the best of our knowledge this (740 ± 70 μs) is the longest room-temperature lifetime for a triplet excited state BODIPY molecule.[27] The lifetime approaches the 1 ms phosphorescence decay time reported for iodinated BODIPY recorded at 77 K.[28]

The short τ_t could reflect a small population of BODIPY dye molecules in the micelles that are more mobile or more readily quenched because they reside in a less-viscous and oxygen-accessible environment at the shell-water interface.[10] We ruled out the possibility that the shorter triplet lifetime was from aqueous dye aggregates in solution because their sandwich-like molecular packing would result in TTA much faster than the tens of μs. Whether the short τ_t is a result of increased TTA, or possibly because of quenching by residual oxygen was unclear from these experiments.

The μs-TA spectroscopy, though preliminary, provides an important insight into the distribution of dye molecules in the micelles, and corroborates our view of the system based on steady-state absorbance spectroscopy. Applications that may benefit from long lived triplet states, such as we recorded in the micelle-encapsulated BODIPY, include TTA upconversion,[27, 50] photoredox catalysis in organic chemistry,[51] and photosensitization for generation of singlet oxygen.[52] An interesting avenue for further study, that might benefit some of the aforementioned applications, is tailoring of the micellar microviscosities through chemical modifications of the constituent polymers in order to achieve specific triplet lifetimes with encapsulated dyes. Alternatively, oxygen penetration and dye mobility can be modified using nanoparticle architectures with buried hydrophilic and hydrophobic domains, such as large compound or bicontinuous micelles.[3]

Conclusions

This study included a characterization of select photophysical properties of an alkoxy-phenyl 2,6-diiodo BODIPY molecule as a function of aggregation state and solvent properties. The ratio of the 0–0 and 0–1 absorption bands of the dye, or A_{ratio}, was used to monitor its state of aggregation, and therefore partitioning into polynorbornene micelles. A_{ratio} is found to be a convenient handle for assessing the propensity of nanomaterials to encapsulate hydrophobic molecules. Through these studies, we conclude the polynorbornene micellar nanoparticles are capable of encapsulating a relatively large hydrophobic molecule, with loadings as high as one dye per ten polymers. Encapsulation efficiencies of the polynorbornene micelles increase with polymer hydrophilicity. A μs-TA investigation of the micelle-encapsulated dye revealed two decay times for the triplet excited state of BODIPY. We tentatively attribute the decay times to populations of dyes that are in the inner and outer corona of the micelles. The longer of the two decay times, 740 μs, is the longest lifetime for a triplet excited state of a BODIPY molecule recorded at room temperature.

Supplementary Material

Refer to Web version on PubMed Central for supplementary material.

Acknowledgments

REFERENCES

1. Holder SJ, Sommerdijk NAJM. New micellar morphologies from amphiphilic block copolymers: disks, toroids and bicontinuous micelles. Polym. Chem. 2011; 2(5):1018–1028.

2. Smart T, Lomas H, Massignani M, Flores-Merino MV, Perez LR, Battaglia G. Block copolymer nanostructures. Nano Today. 2008; 3(3-4):38–46.

3. Barnhill SA, Bell NC, Patterson JP, Olds DP, Gianneschi NC. Phase Diagrams of Polynorbornene Amphiphilic Block Copolymers in Solution. Macromolecules. 2015

4. Rao NV, Mane S, Kishore A, Das Sarma J, Shunmugam R. Norbornene Derived Doxorubicin Copolymers as Drug Carriers with pH Responsive Hydrazone Linker. Biomacromolecules. 2012; 13(1):221–230. [PubMed: 22107051]

5. Rush AM, Thompson MP, Tatro ET, Gianneschi NC. Nuclease-Resistant DNA via High-Density Packing in Polymeric Micellar Nanoparticle Coronas. ACS Nano. 2013; 7(2):1379–1387. [PubMed: 23379679]

6. Chien M-P, Thompson MP, Barback CV, Ku T-H, Hall DJ, Gianneschi NC. Enzyme-Directed Assembly of a Nanoparticle Probe in Tumor Tissue. Adv. Mater. 2013; 25(26):3599–3604. [PubMed: 23712821]

7. Bertin PA, Gibbs JM, Shen CK-F, Thaxton CS, Russin WA, Mirkin CA, Nguyen ST. Multifunctional polymeric nanoparticles from diverse bioactive agents. Journal of the American Chemical Society. 2006; 128(13):4168–4169. [PubMed: 16568958]

8. Xu J, Fu Q, Ren JM, Bryant G, Qiao GG. Novel drug carriers: from grafted polymers to cross-linked vesicles. Chemical Communications. 2013; 49(1):33–35. [PubMed: 23124220]

9. Lim Soo P, Eisenberg A. Preparation of block copolymer vesicles in solution. J. Polym. Sci. Pol. Phys. 2004; 42(6):923–938.

10. Webber SE. Polymer Micelles: An Example of Self-Assembling Polymers. J. Phys. Chem. B. 1998; 102(15):2618–2626.

11. Proetto MT, Rush AM, Chien M-P, Abellan Baeza P, Patterson JP, Thompson MP, Olson NH, Moore CE, Rheingold AL, Andolina C, Millstone J, Howell SB, Browning ND, Evans JE, Gianneschi NC. Dynamics of Soft Nanomaterials Captured by Transmission Electron Microscopy in Liquid Water. J. Am. Chem. Soc. 2014; 136(4):1162–1165. [PubMed: 24422495]

12. Bertin PA, Watson KJ, Nguyen ST. Indomethacin-containing nanoparticles derived from amphiphilic polynorbornene: a model ROMP-based drug encapsulation system. Macromolecules. 2004; 37(22):8364–8372.

13. Liu Y, Piñón V, Weck M. Poly (norbornene) block copolymer-based shell cross-linked micelles with Co (III)–salen cores. Polymer Chemistry. 2011; 2(9):1964–1975.

14. Ogawa S, Takano S, Fujimori H, Itoh T, Kaita S, Iida T, Wakatsuki Y. Ring-opening metathesis polymerization of steroid-conjugated norbornenes and gradual release of estrone from a polymer film. Reactive and Functional Polymers. 2010; 70(9):563–571.

15. Lim Soo P, Luo L, Maysinger D, Eisenberg A. Incorporation and Release of Hydrophobic Probes in Biocompatible Polycaprolactone-block-poly(ethylene oxide) Micelles: Implications for Drug Delivery. Langmuir. 2002; 18(25):9996–10004.

16. Letchford K, Liggins R, Burt H. Solubilization of hydrophobic drugs by methoxy poly(ethylene glycol)-block-polycaprolactone diblock copolymer micelles: Theoretical and experimental data and correlations. J. Pharm. Sci. 2008; 97(3):1179–1190. [PubMed: 17683080]

17. Kwon GS, Naito M, Kataoka K, Yokoyama M, Sakurai Y, Okano T. Block copolymer micelles as vehicles for hydrophobic drugs. Colloid Surface B. 1994; 2(4):429–434.

18. Njikang G, Gauthier M, Li J. Arborescent polystyrene-graft-poly(2-vinylpyridine) copolymers as unimolecular micelles: Solubilization studies. Polymer. 2008; 49(5):1276–1284.

19. Wilhelm M, Zhao CL, Wang Y, Xu R, Winnik MA, Mura JL, Riess G, Croucher MD. Poly(styrene-ethylene oxide) block copolymer micelle formation in water: a fluorescence probe study. Macromolecules. 1991; 24(5):1033–1040.

20. López Arbeloa F, Bañuelos J, Martínez V, Arbeloa T, López Arbeloa I. Structural, photophysical and lasing properties of pyrromethene dyes. Int. Rev. Phys. Chem. 2005; 24(2):339–374.

21. Poe AM, Della Pelle AM, Subrahmanyam AV, White W, Wantz G, Thayumanavan S. Small molecule BODIPY dyes as non-fullerene acceptors in bulk heterojunction organic photovoltaics. Chem. Commun. 2014; 50(22):2913–2915.

22. Yang Y, Guo Q, Chen H, Zhou Z, Guo Z, Shen Z. Thienopyrrole-expanded BODIPY as a potential NIR photosensitizer for photodynamic therapy. Chem. Commun. 2013; 49(38):3940–3942.

23. Kamkaew A, Lim SH, Lee HB, Kiew LV, Chung LY, Burgess K. BODIPY dyes in photodynamic therapy. Chem. Soc. Rev. 2013; 42(1):77–88. [PubMed: 23014776]

24. Awuah SG, You Y. Boron dipyrromethene (BODIPY)-based photosensitizers for photodynamic therapy. RSC Advances. 2012; 2(30):11169–11183.

25. Ulrich G, Ziessel R, Harriman A. The chemistry of fluorescent bodipy dyes: versatility unsurpassed. Angew. Chem. Int. Ed. 2008; 47(7):1184–1201.

26. Benniston AC, Copley G. Lighting the way ahead with boron dipyrromethene (Bodipy) dyes. Phys. Chem. Chem. Phys. 2009; 11(21):4124–4131. [PubMed: 19458813]

27. Wu W, Guo H, Wu W, Ji S, Zhao J. Organic Triplet Sensitizer Library Derived from a Single Chromophore (BODIPY) with Long-Lived Triplet Excited State for Triplet–Triplet Annihilation Based Upconversion. J. Org. Chem. 2011; 76(17):7056–7064. [PubMed: 21786760]

28. Sabatini RP, McCormick TM, Lazarides T, Wilson KC, Eisenberg R, McCamant DW. Intersystem Crossing in Halogenated Bodipy Chromophores Used for Solar Hydrogen Production. J. Phys. Chem. Lett. 2011; 2(3):223–227.

29. Zhai D, Agrawalla BK, Eng PSF, Lee S-C, Xu W, Chang Y-T. Development of a fluorescent sensor for an illicit date rape drug - GBL. Chem. Commun. 2013; 49(55):6170–6172.

30. Nagai A, Kokado K, Miyake J, Cyujo Y. Thermoresponsive fluorescent water-soluble copolymers containing BODIPY dye: Inhibition of H-aggregation of the BODIPY units in their copolymers by LCST. J. Polym. Sci. Pol. Chem. 2010; 48(3):627–634.

31. Ortiz MJ, Agarrabeitia AR, Duran-Sampedro G, Bañuelos Prieto J, Lopez TA, Massad WA, Montejano HA, García NA, Lopez Arbeloa I. Synthesis and functionalization of new polyhalogenated BODIPY dyes. Study of their photophysical properties and singlet oxygen generation. Tetrahedron. 2012; 68(4):1153–1162.

32. Popere BC, Della Pelle AM, Thayumanavan S. BODIPY-Based Donor–Acceptor π-Conjugated Alternating Copolymers. Macromolecules. 2011; 44(12):4767–4776.

33. Zhang C, Zhao J, Wu S, Wang Z, Wu W, Ma J, Guo S, Huang L. Intramolecular RET Enhanced Visible Light-Absorbing Bodipy Organic Triplet Photosensitizers and Application in Photooxidation and Triplet–Triplet Annihilation Upconversion. J. Am. Chem. Soc. 2013; 135(28): 10566–10578. [PubMed: 23790008]

34. Pozdnyakov IP, Aksenova YV, Ermolina EG, Melnikov AA, Kuznetsova RT, Grivin VP, Plyusnin VF, Berezin MB, Semeikin AS, Chekalin SV. Photophysics of diiodine-substituted fluorinated boron–dipyrromethene: A time resolved study. Chem. Phys. Lett. 2013; 585(0):49–52.

35. Chien MP, Rush AM, Thompson MP, Gianneschi NC. Programmable Shape-Shifting Micelles. Angewandte Chemie International Edition. 2010; 49(30):5076–5080.

36. Hahn ME, Randolph LM, Adamiak L, Thompson MP, Gianneschi NC. Polymerization of a peptide-based enzyme substrate. Chemical Communications. 2013; 49(28):2873–2875. [PubMed: 23450132]

37. Sanford MS, Love JA, Grubbs RH. A Versatile Precursor for the Synthesis of New Ruthenium Olefin Metathesis Catalysts. Organometallics. 2001; 20(25):5314–5318.

38. Adams DJ, Kitchen C, Adams S, Furzeland S, Atkins D, Schuetz P, Fernyhough CM, Tzokova N, Ryan AJ, Butler MF. On the mechanism of formation of vesicles from poly(ethylene oxide)-block-poly(caprolactone) copolymers. Soft Matter. 2009; 5(16):3086–3096.

39. Wang, C.; Angelella, M.; Kuo, C-H.; Tauber, MJ. Singlet fission in carotenoid aggregates: insights from transient absorption spectroscopy. SPIE; 2012. Physical Chemistry of Interfaces and Nanomaterials XI. 845905-845905-13

40. Kasha M, Rawls HR, Ashraf El-Bayoumi M. The exciton model in molecular spectroscopy. Pure Appl. Chem. 1965; 11:371.

41. Spano FC. The Spectral Signatures of Frenkel Polarons in H- and J-Aggregates. Accounts Chem. Res. 2010; 43(3):429–439.

42. Alamiry MAH, Benniston AC, Copley G, Harriman A, Howgego D. Intramolecular Excimer Formation for Covalently Linked Boron Dipyrromethene Dyes. J. Phys. Chem. A. 2011; 115(44): 12111–12119. [PubMed: 21951157]

43. Benniston AC, Copley G, Harriman A, Howgego D, Harrington RW, Clegg W. Cofacial Boron Dipyrromethene (Bodipy) Dimers: Synthesis, Charge Delocalization, and Exciton Coupling. J. Org. Chem. 2010; 75(6):2018–2027. [PubMed: 20155975]

44. Saki N, Dinc T, Akkaya EU. Excimer emission and energy transfer in cofacial boradiazaindacene (BODIPY) dimers built on a xanthene scaffold. Tetrahedron. 2006; 62(11):2721–2725.

45. Mikhalyov I, Gretskaya N, Bergstrom F, Johansson LBA. Electronic ground and excited state properties of dipyrrometheneboron difluoride (BODIPY): Dimers with application to biosciences. Phys. Chem. Chem. Phys. 2002; 4(22):5663–5670.

46. Bergström F, Mikhalyov I, Hägglöf P, Wortmann R, Ny T, Johansson LBÅ. Dimers of Dipyrrometheneboron Difluoride (BODIPY) with Light Spectroscopic Applications in Chemistry and Biology. J. Am. Chem. Soc. 2002; 124(2):196–204. [PubMed: 11782171]

47. Vargas J, Martínez A, Santiago AA, Tlenkopatchev MA, Gaviño R, Aguilar-Vega M. The effect of fluorine atoms on gas transport properties of new polynorbornene dicarboximides. J. Fluorine Chem. 2009; 130(2):162–168.

48. Cheng G, Hua F, Melnichenko YB, Hong K, Mays JW, Hammouda B, Wignall GD. Conformation of oligo (ethylene glycol) grafted poly (norbornene) in solutions: A small angle neutron scattering study. Eur. Polym. J. 2008; 44(9):2859–2864.

49. Weber G, Shinitzky M, Dianoux AC, Gitler C. Microviscosity and order in the hydrocarbon region of micelles and membranes determined with fluorescent probes. I. Synthetic micelles. Biochemistry-US. 1971; 10(11):2106–2113.

50. Singh-Rachford TN, Castellano FN. Photon upconversion based on sensitized triplet–triplet annihilation. Coord. Chem. Rev. 2010; 254(21-22):2560–2573.

51. Guo S, Zhang H, Huang L, Guo Z, Xiong G, Zhao J. Porous material-immobilized iodo-Bodipy as an efficient photocatalyst for photoredox catalytic organic reaction to prepare pyrrolo[2,1-a]isoquinoline. Chem. Commun. 2013; 49(77):8689–8691.

52. Yogo T, Urano Y, Ishitsuka Y, Maniwa F, Nagano T. Highly Efficient and Photostable Photosensitizer Based on BODIPY Chromophore. J. Am. Chem. Soc. 2005; 127(35):12162–12163. [PubMed: 16131160]
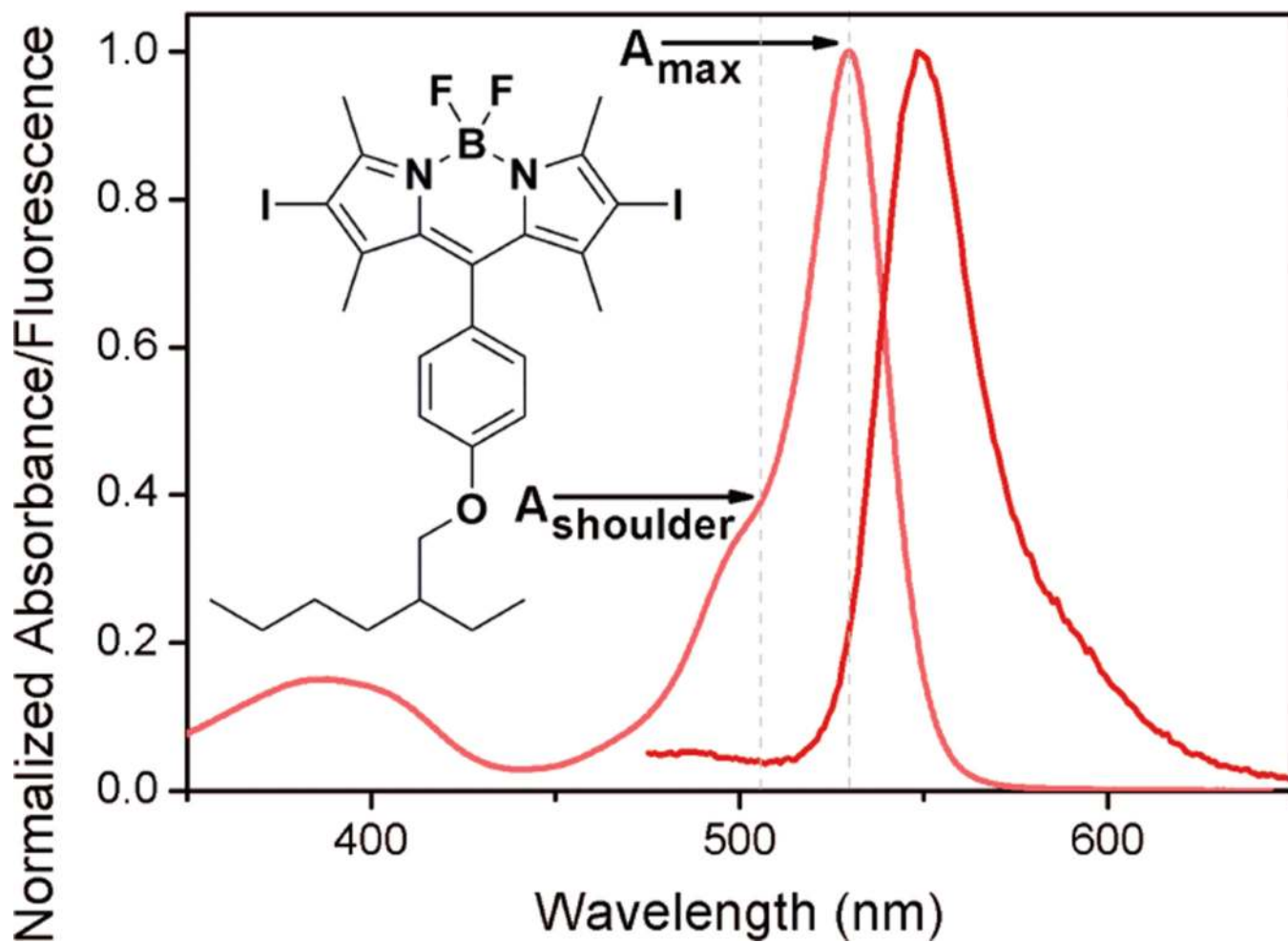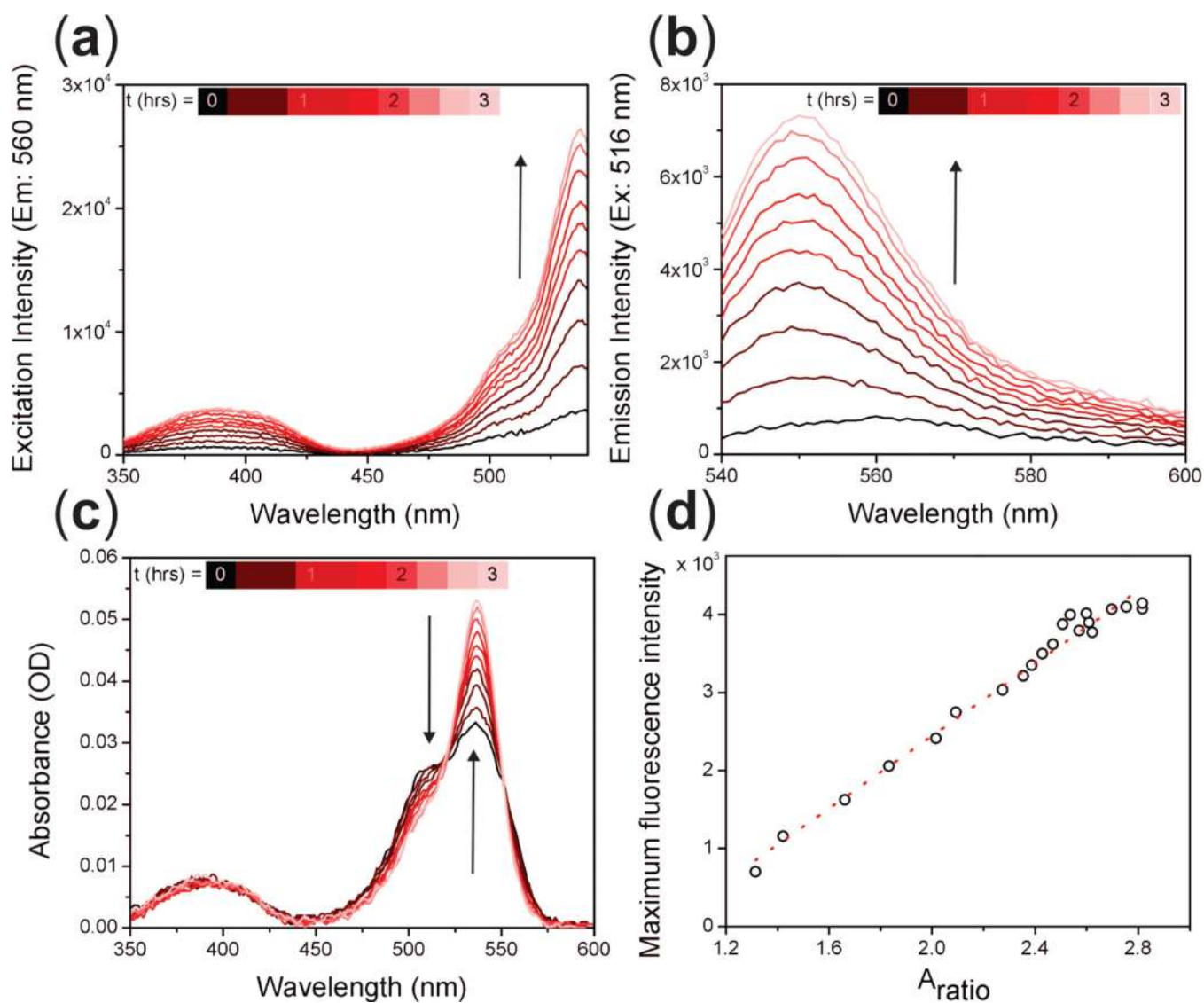
Figure 1.
Alkoxy-phenyl 2,6-diiodo BODIPY molecule (inset), with normalized absorbance and
fluorescence spectra of the molecule in acetone.
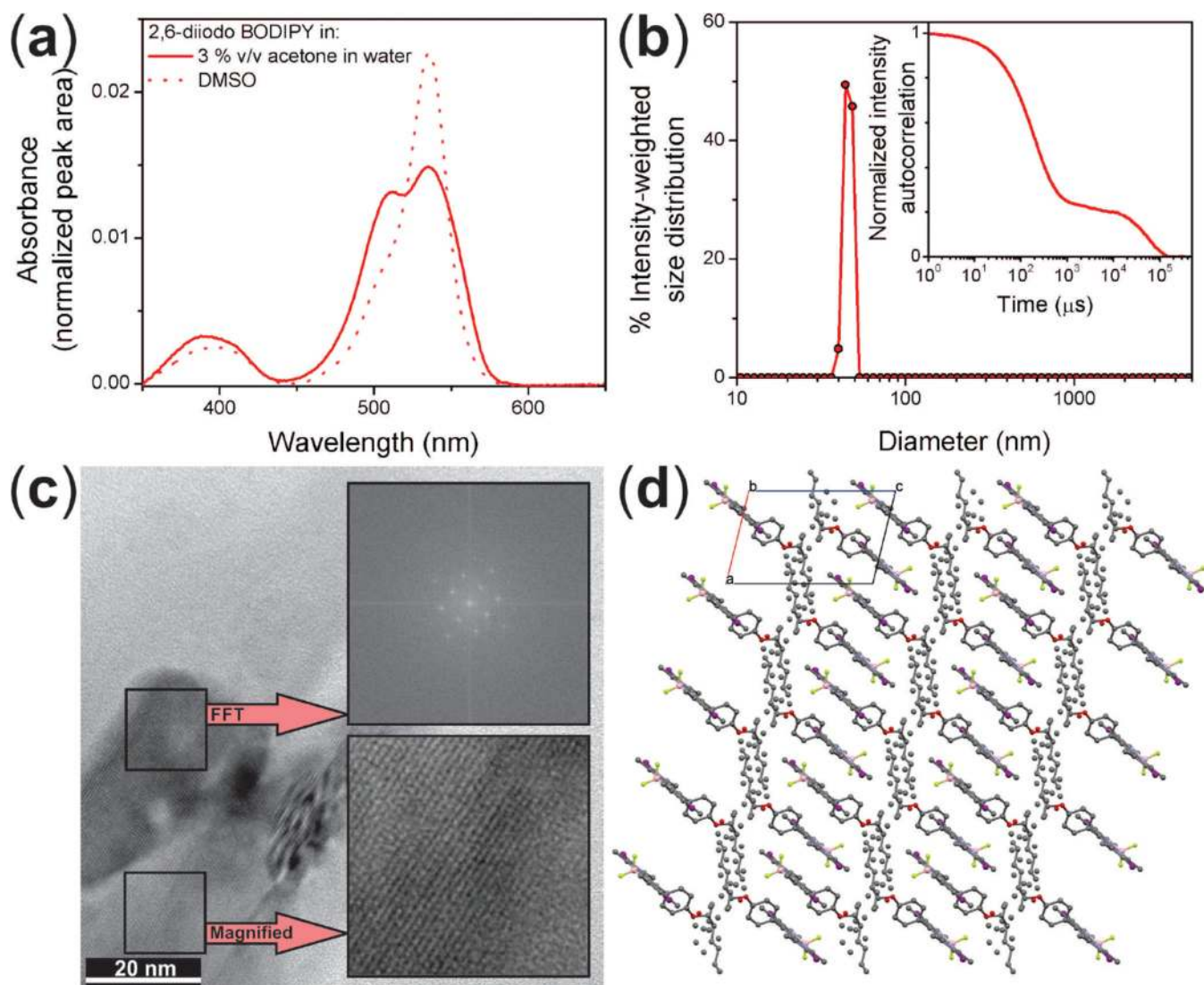
Figure 2.
Characterization of BODIPY dye aggregates in aqueous environments. (**a**) Absorbance spectra of 2,6-diiodo BODIPY aggregated in majority water (3 % v/v acetone) versus solvated in DMSO. (**b**) DLS measurements (**c**) dry-state TEM images of a 2.5 μM aqueous (3 % v/v acetone) dye solution. (**d**) Anti-parallel dimer formation determined by X-ray crystallography.
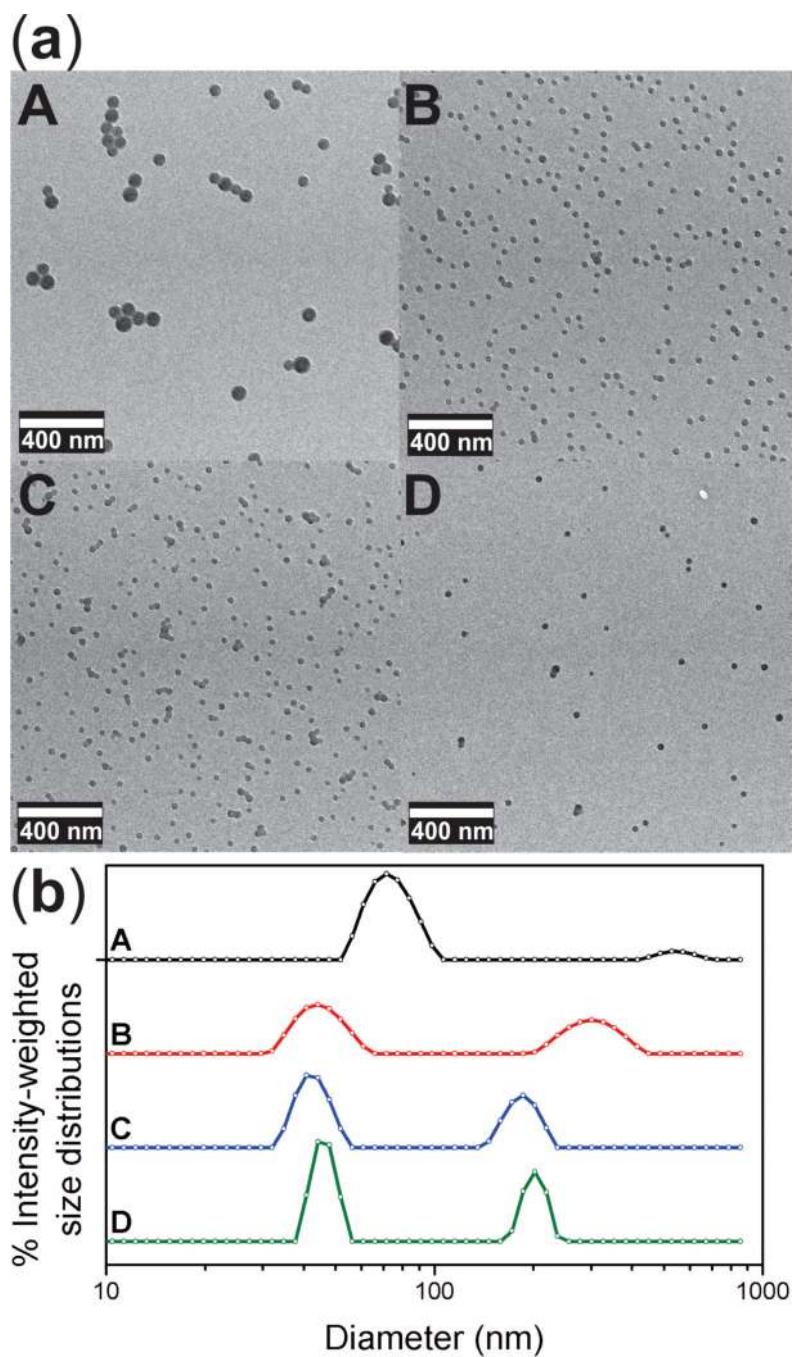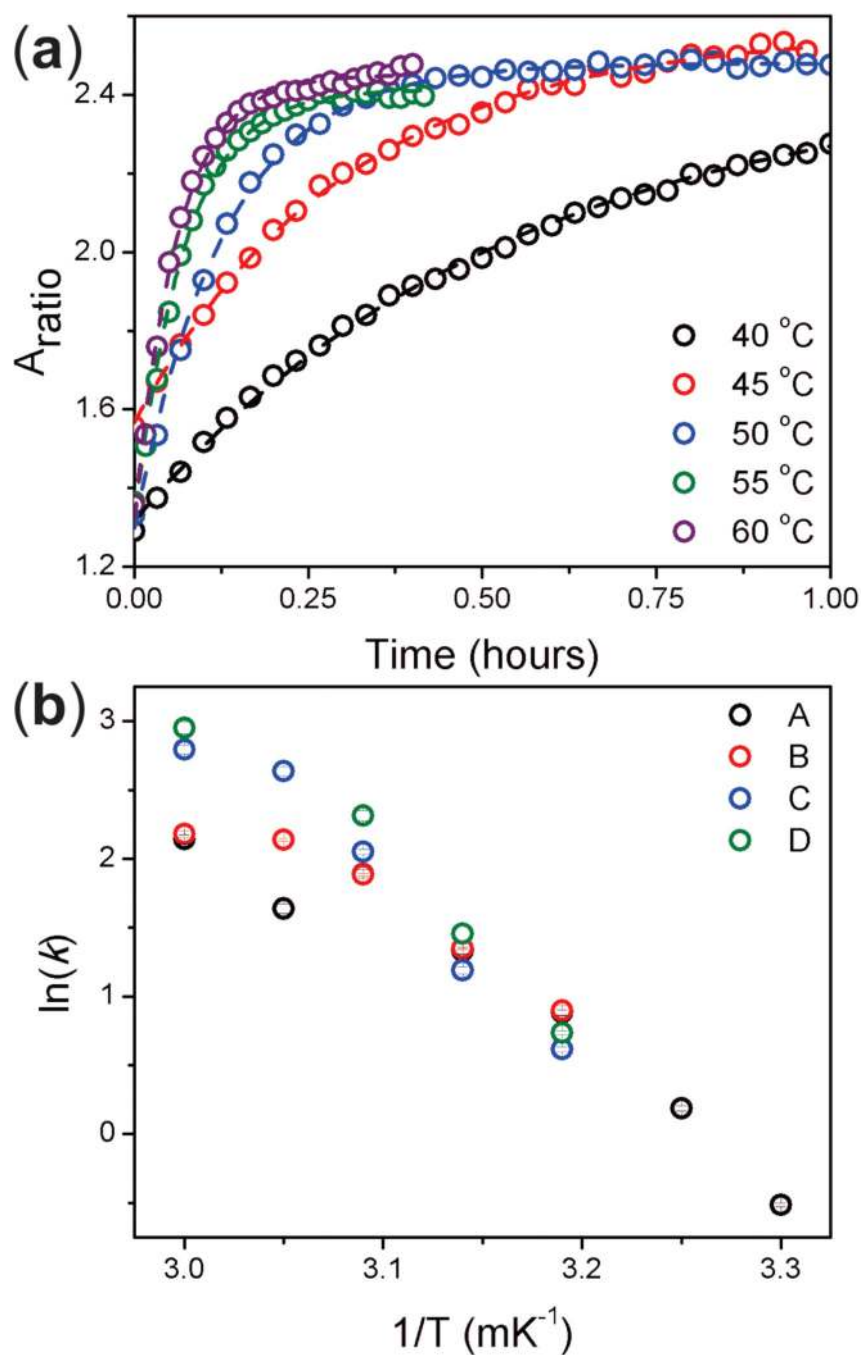
Figure 3.
Micelle characterization including (**a**) TEM images of micelles formulated from polymers A to D and (**b**) results from DLS measurements, which indicate that each polymer sample forms both agglomerated and dispersed micelles in water.
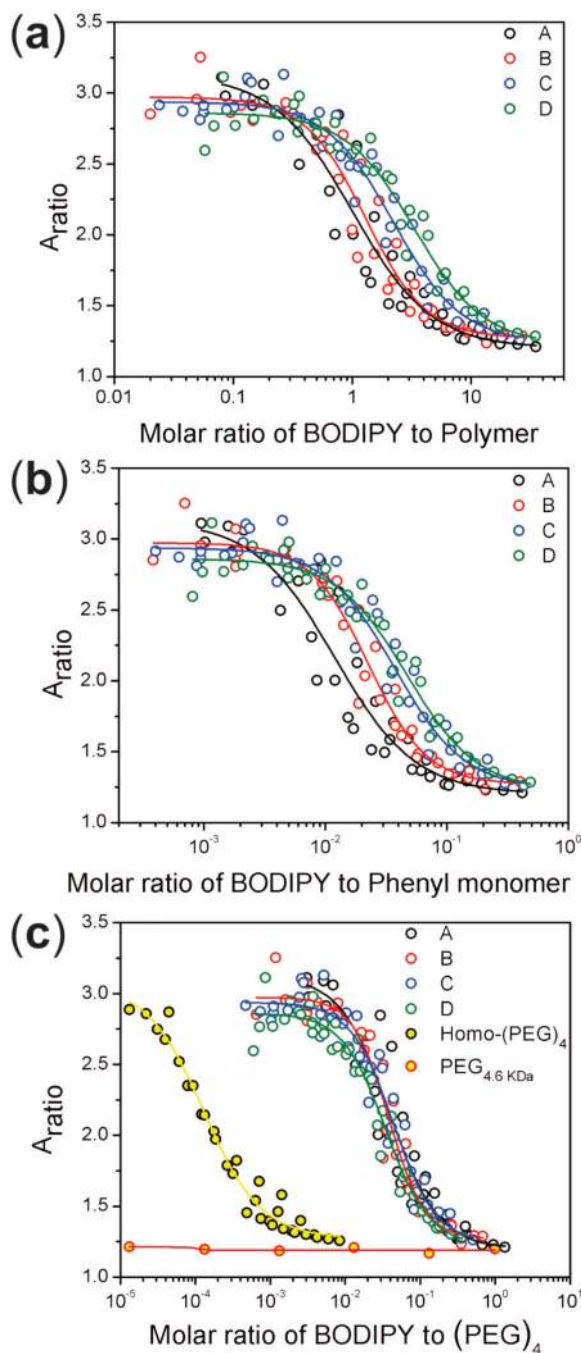
Figure 4.
(**a**) Fluorescence excitation, (**b**) emission, and (**c**) absorbance spectra of 2,6-diiodo BODIPY in the presence of polymer B micelles in water with 3 % v/v acetone, over a 3 hour period at room temperature. (**d**) Linear relationship between fluorescence intensity and A_{ratio} (adj. R^2 = 0.98).
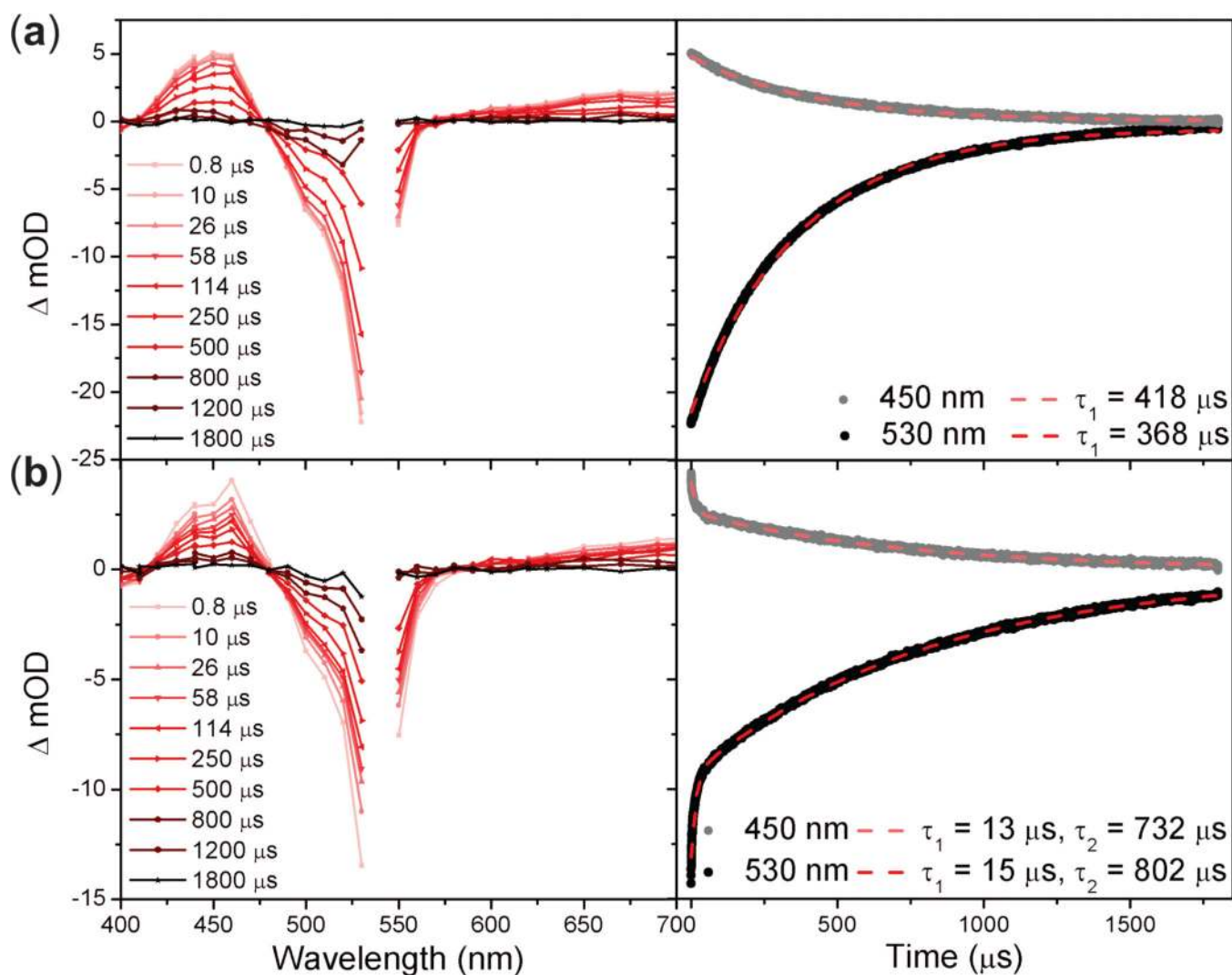
Figure 5.
(**a**) Time-dependent changes in the A_{ratio} of 2,6-diiodo BODIPY in the presence of polymer C micelles, at temperatures between 40 °C and 60 °C in water with 3 % v/v acetone. The data are fitted with single exponential functions. (**b**) Arrhenius plots of the rate of dye encapsulation by polymer micelles A – D.

Figure 6.
(**a**) Dependence of A_{ratio}, measured after 1 hour at 50 °C, on the relative amounts of dye and polymer in solution. The same data are also presented as a function of the ratio of dye to phenyl monomer (**b**) and (PEG)$_4$ monomer (**c**). Also plotted in (**c**) are the A_{ratios} observed in solutions of the dye with the homopolymer of (PEG)$_4$ (Homo-(PEG)$_4$) and in solutions of the dye with 4.6 kDa poly(ethylene) glycol (PEG$_{4.6kDa}$). All measurements carried out in water with 3 % v/v acetone. For the data in Figures 6 (b) and (c) plotted on the same x-axis see Figure S12.
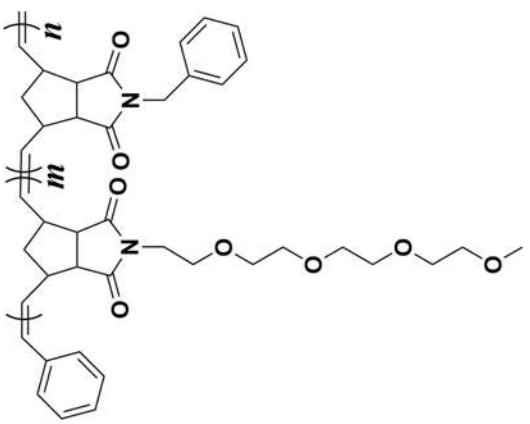
Figure 7.
Transient absorption data for (**a**) 2.5 μM BODIPY solution in toluene, and (**b**) micelle encapsulated BODIPY solution. Data at 540 nm were omitted from the spectra because of pump scattering. The right-hand panels show the recovery of the ground state bleach at 530 nm, and decay of triplet excited state at 450 nm, fitted with a single or double exponential function. The decay times of the triplet excited state (averaged over 440 nm, 450 nm and 460 nm) and the recovery of the ground state bleach (averaged over 500 nm, 510 nm and 520 nm) were matched, within the uncertainty of the measurement, see Table S5.

Table 1

Summary of the polynorbornene polymer characteristics.

Polymer	m	n	M_N (kDa)	M_W/M_N	X_m	Chemical Structure
A	26	84	30	1.08	0.24	
B	37	63	29	1.06	0.37	
C	51	60	33	1.10	0.46	
D	96	71	52	1.17	0.57	
E	77	38	37	1.01	0.67	
Homo–(PEG)$_4$	85	0	31	1.04	1.00	

$((PEG)_4)_m$-b-(phenyl)$_n$